Study of aluminum - iron oxide composites obtained by die pressing of industrial by-products

A. Esguerra-Arce[1]*, G. Pinto-Arciniegas[1], S. Silva-Hurtado[1], R. Setchi[2], J. Esguerra-Arce[1]

[1]CIMSER, Escuela Colombiana de Ingeniería Julio Garavito, Bogotá, Colombia. Code 57

[2]High-Value Manufacturing, Cardiff University, Cardiff, United Kingdom. Code 44

*Corresponding author, E-mail: adriana.esguerra@escuelaing.edu.co

Postal address: Escuela Colombiana de Ingeniería Julio Garavito, AK 45 No 205-59 (Autopista Norte) P. C. 111166, Bogotá.

Abstract

In cities in developing countries several tons of unprocessed aluminum are buried every day. This is because some kinds of aluminum by-products exhibit low recyclability through remelting, as is the case with sawn mechanical chips. Therefore, the purpose of this project was to address the problem of aluminum chips recycling. The technical approach included the development of a reinforced aluminum with mill scale, an iron oxide by-product from the high-temperature rolling of steel. Aluminum chips and mill scale were first ground separately and the resulting powders characterized. Next, the powders were mixed at different percentages of mill scale (0%, 0.5%, 1.0%, and 2.0 %), compacted, and sintered in a protective atmosphere. Iron oxide-aluminum composites were characterized by optical and scanning electron microscopy, X ray diffraction, differential scanning calorimetry, hardness tests and potentiodynamic polarization test. The iron oxide particles and aluminum matrix produced a thermite reaction, forming different kinds of interfaces as a function of the quantity of mill scale. It was found that 0.5% of mill scale is the optimal value for addition, because it improves the hardness of the composite from 50.0 ± 2.4 HRF to 99.9 ± 2.5 HRF. The corrosion rate decreased from 496.7 to 21.0 µm/year.

Key words

Recycling, aluminum, powder metallurgy, thermite reaction, industrial by-products, sustainability

1. Introduction

1.1. Importance of recycling industrial by-products

Most manufacturing processes produce waste. This is the case with iron and steel manufactured at high temperatures by plastic deformation, as well as with machined metal pieces produced by milling. However, one of the greatest current global challenges is combining environmental sustainability with economic growth. This is the objective of the 12th Sustainable Development Goal of responsible production, which invites us to do more and better with less by efficiently using natural resources and reducing waste generation through recycling [**1**]. Although parts of the world have progressed in this area, humanity is not yet able to meet the challenge of producing zero waste. In Colombia, some areas have a lag in the recycling of materials compared to the maximum reference worldwide.

The policy of Sustainable Production and Consumption, as well as CONPES 3874, which defines the national politicies for the Integral Management of Solid Wastes, provided the basis for Colombia to begin its transition to becoming a circular economy [**2**]. This is the case for all countries in Latin America. However, despite these policy developments, the internal demand for materials in the country has grown rapidly, driven by increasing use of minerals for construction. This reveals the need to advance and strengthen the implementation of technologies with cleaner processes that allow the reuse of materials in production cycles, as well as reductions in the generation of waste.

Given that mill scale and machining chips are two very important industrial by-products that are generated in great quantities, efforts are being made by researchers to reintegrate these into the production chain through innovative manufacturing techniques that are suitable for the

circular economy. In this case, two research groups, from the United Kingdom (UK) and Colombia, are working together under an Industry-Academia Partnership Program of the Royal Academy of Engineering.

1.2. Industrial by-products: iron oxide mill scale and aluminum chips

Mill scale is produced in steel making, during the casting and rolling processes. When steel is heated, mill scale is formed on its surface due to the interaction between hot steel and ambient oxygen. Mill scale is composed of three kinds of iron oxide: wüstite (FeO), magnetite (Fe_3O_4), and hematite (Fe_2O_3) [**3**]. This iron oxide is not a protective oxide, so it detaches from the steel, permitting the diffusion of oxygen molecules, which in turn cause the corrosive process to continue. Therefore, during the manufacturing process, mill scale is mechanically removed. Steel-making plants in Colombia produce huge volumes of this by-product, which is sold for various purposes, including for iron production in countries such as China and Peru; as an addition to cement clinker; and for use in ferro-alloys and counterweights [**4**].

Meanwhile, machining chips are produced in considerable quantities as waste from sawing, which is the most common technique used to cut metals in manufacturing processes. These chips are small and semi-continuous, so they are not suitable for recycling by melting, because no more than 54% are recovered [**5**, **6**]. This fact prompted a research project in which recycled aluminum saw chips were ground and processed by powder metallurgy techniques (compacting and sintering), achieving highly positive results, as "obtained samples exhibited 95% of pre-sawing original aluminum hardness" [**7**].

1.3. Aluminum-iron oxide composites

Some studies have been conducted on iron oxide reinforced aluminum, with different research focuses. Vibration properties of Al-Fe_2O_3 were studied by Shivakumar et al. [**8**], finding that Al-4% Fe_2O_3 shows more improvement in dynamic properties than pure aluminum (Al). Bayraktar and Katundi [**9**] developed an Al-Fe_3O_4 composite with improved conductivity and magnetic

properties. They found that green density and hardness increased with iron oxide content. The optimal percentage reported was 8% of Fe_3O_4. Other studies combined Fe_2O_3 with other compounds, such as carbon nanotubes [**10**] and boron carbide [**11**] to produced reinforced aluminum.

With regard to thermodynamic aspects, it is known that aluminum acts as a reducing agent for iron oxide, as can be inferred by the schematic Ellingham diagram shown in **Fig. 1**. Therefore, when iron oxide particles are added to an aluminum matrix, redox reactions take place at high temperatures. The oxidation reaction of aluminum exhibits lower Gibbs-free energy than the oxidation reaction of iron, leading to the chemical reduction of iron oxides and the chemical oxidation of aluminum. This kind of chemical reaction is called a thermite reaction, which is in the form $A + BO \rightarrow AO + B + heat$.

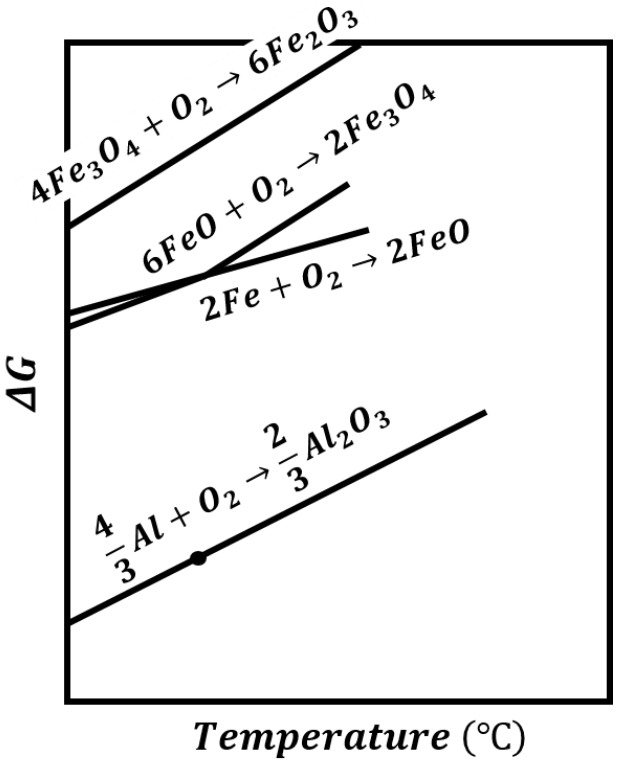

Fig. 1. Ellingham diagram showing the temperature dependence of the stability of aluminum, iron, and their respective oxides.

It is expected that these chemical reactions, which occur at the interface between aluminum and iron oxide particles, will generate an interface between reinforcing particles and the matrix, improving mechanical strength. However, the system must be analyzed and the products of the reaction studied. For example, the presence of iron in aluminum alloys has been recognized as detrimental due to the formation of iron-rich intermetallics, which induces stress and initiate cracks [**12 - 13**].

1.4. Thermite reaction

The Fe_2O_3/Al thermite reaction has been studied since the 1970s, although the information available on Fe_3O_4/Al or FeO/Al is not extensive. Regarding the reaction with Fe_2O_3, Duraes *et al* [**14**] provided a good state-of-the-art report in 2007. In their study, they proposed a qualitative mechanism for the thermite reaction in the mode of self-propagating high temperatures, i.e., at temperatures when aluminum is liquid:

1. In the ignition period, Fe_2O_3 is reduced to Fe_3O_4 and FeO;
2. Released oxygen reacts with the melted aluminum (melted or vaporized), forming alumina and releasing high amounts of heat; and
3. Alumina and hercynite ($FeO \cdot Al_2O_3$) grains are formed.

1.5. Objectives

Considering the above, the aim of this paper was to evaluate whether it is possible to manufacture iron oxide-reinforced aluminum composites based on two important industrial by-products: mill scale and sawn aluminum chips. The manufacturing technique used in this stage of the project was powder metallurgy, i.e. the compacting and sintering of powders. The influence of iron oxide quantity on the hardness and microstructure of the composites was analyzed.

2. Materials and Methods

2.1. Preparation of the powders

Chips were obtained from a 6xxx Al alloy (Al-Mg-Si) of 49 HRF, which was machined with a mechanical saw in the production laboratory of our academic institution (Colombian School of Engineering Julio Garavito). Mill scale derived from the rolling production of low carbon steel was obtained from the Colombian steel-making business Gerdau-Diaco. Each of the materials was ground separately. Taking into account one of our previous studies [**7**], aluminum chips were ground for 56 hours in a ball mill using zirconia grinding bodies and a rotational speed of 55 rpm. The grinding bodies to material volumetric ratio was 10:1. The mill scale was ground for 95 hours using steel balls as grinding bodies at 55 rpm, using a grinding bodies to material volumetric ratio of 4:6.

2.2. Characterization of the powders

Powders were characterized by scanning electron microscopy (SEM), laser granulometry, and X-ray diffraction (XRD) in order to observe the morphology, particle size and size distribution, and crystalline phases in the materials, respectively. The SEM used was coupled to an energy dispersive X-ray spectroscope (JEOL JSM-649 OLV). The laser granulometer used was a Hydro 2000MU (A) device, using water as dispersant. XRD was performed with a Brucker D8 Discover, using a Cu target. Phase identification was performed using X'Pert HighScore software.

2.3. Compaction and sintering processes

To evaluate the influence of iron oxide powder on aluminum hardness, mechanical mixings of aluminum with iron oxide powder at 0, 0.5, 1.0, and 2.0 weight% were performed for 1 hour at 30 rpm. Pieces (12.7 mm in diameter and 6 mm in height) were obtained by compaction. Cold compaction was performed using an Eneparc 50 Ton uniaxial hydraulic press and H13 steel molds and punches, which prior to this were impregnated with magnesium stearate as a lubricant. The applied load was 19000 lbf, equivalent to 800 MPa, which was applied for 30 seconds. Next, cylindrical samples were sintered in a steel chamber in the presence of Ar at 620

°C for 1 hour, using a heating rate of 5 °C/min. At this point, in order to evaluate the presence of thermite reaction, 60 mg samples of Al-0% MS and Al-1% MS were compacted under the same conditions mentioned before, then divided in 4 parts, each of which was submitted to thermogravimetry – TGA and differential scanning calorimetry - DSC analysis. The conditions of the tests were an inert atmosphere of nitrogen, and a heating rate of 10 °C/min, going from room temperature to 630 °C. The equipment used was a SDT Q600 V20.9 Build 20.

2.4. Characterization of the sintered pieces

Sintered samples were characterized by optical microscopy and SEM to observe the iron oxide particle distribution in the aluminum matrix as well as the formed interface, and by XRD for the analysis of crystalline phases. Hardness behavior was analyzed with a digital durometer (Gnehm Harteprufer), using an RF scale (ball indenter of 1/16'' and 60 kg of load) for the measurements. Five measurements were made in three samples for each concentration. Corrosion behavior of the Al-0MS and higher hardness samples with mill scale were evaluated. Potentiodynamic polarization test was carried out in 3.5% wt. NaCl solution with a pH of 7. The reference electrode was Ag/AgCl and the counter electrode was graphite. The Al Al-mill scale samples were regarded as working electrodes with 1 cm^2 exposure to the NaCl solution. Corrosion rate was calculated using the following formula [**15**]:

$$v_{corr}(mm/year) = \frac{3270 \times M \times i_{corr}}{\rho \times Z}$$

where 3270 is a constant that defines the unit corrosion rate, M is the atomic mass of the metal (Al), i_{corr} is the corrosion current density, ρ is the density of the metal (Al) and Z is the number of electrons transferred per atom.

3. Results and Discussion

3.1. Powder characterization

The chemical composition of the Al-Mg-Si alloy identified by EDS analysis were 49.08% Al, 27.41% O, 4.28% Si and 1.16% Mg, corroborating the presence of magnesium and silicon in the alloy. The presence of oxygen was also expected, because of the air atmosphere during grinding and the interaction with air atmosphere in general. This indicates that a layer of aluminum oxide was surrounding the aluminum powders. **Fig. 2** -a) shows the XRD pattern and SEM image of the aluminum alloy powder. The XRD pattern shows the typical peaks of aluminum, which corresponded to (111), (200), (220), and (311) planes of the FCC structure (pdf 00-004-0787 of X'Pert HighScore). Other small peaks were observed, which corresponded to alumina (pdf 01-089-0686 of X'Pert HighScore), the aluminum oxide surrounding the particles. No peaks of Mg_2Si were observed, which indicated that there was no precipitation of this compound, but rather a solutionized condition of the alloy [**16**]. The morphology of the particles was rounded, which has been typically observed at high grinding times [**7**]. **Fig. 2** -b) shows the particle size distribution of the aluminum powder. Granulometric curves showed bimodal behaviors of the size distribution, although the largest group corresponded to the finest particles. The average particle size was 42.98 μm.

Crystallographic information obtained by the XRD pattern of the aluminum powder is lattice parameter = 0.40479 nm, and crystallite size = 159 nm. The smaller value of the lattice parameter in comparison to that of the stress-free Al-Mg-Si alloy, which is higher than 0.4094 nm for pure aluminum [**17**], indicates residual compressive stress in the lattice due to the action of the grinding bodies during the milling process.

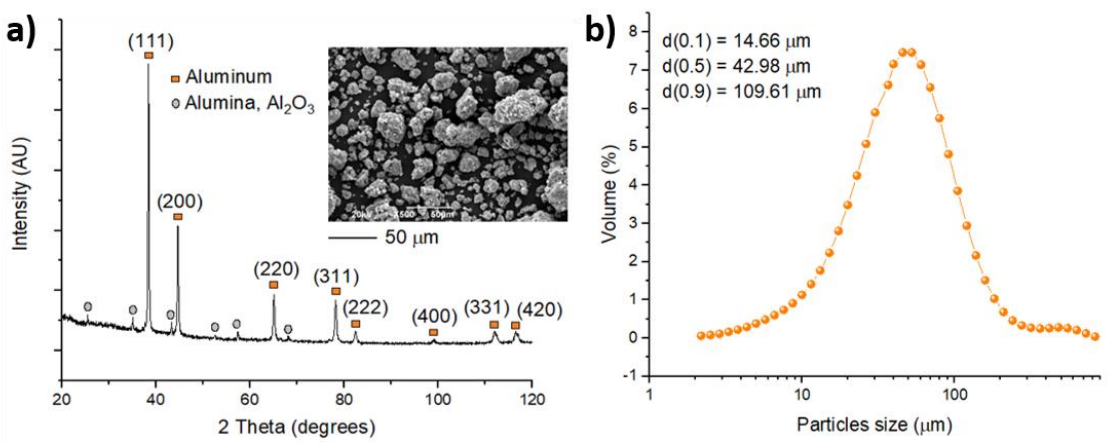

Fig. 2. a) XRD pattern and SEM micrograph of the aluminum alloy powder, b) particle size distribution of the aluminum powder.

Fig. 3 shows the results of the mill scale powder characterization. The particle morphology was rounded and typical of a comminuted ceramic. XRD refinement showed that the mill scale consisted of 4.6% hematite, 29.6% magnetite, and 65.9% wüstite, which is a typical composition of a steel oxide scale [**3**]. The granulometric curve showed monomodal behavior. The mean diameter of the particles was 47 μm.

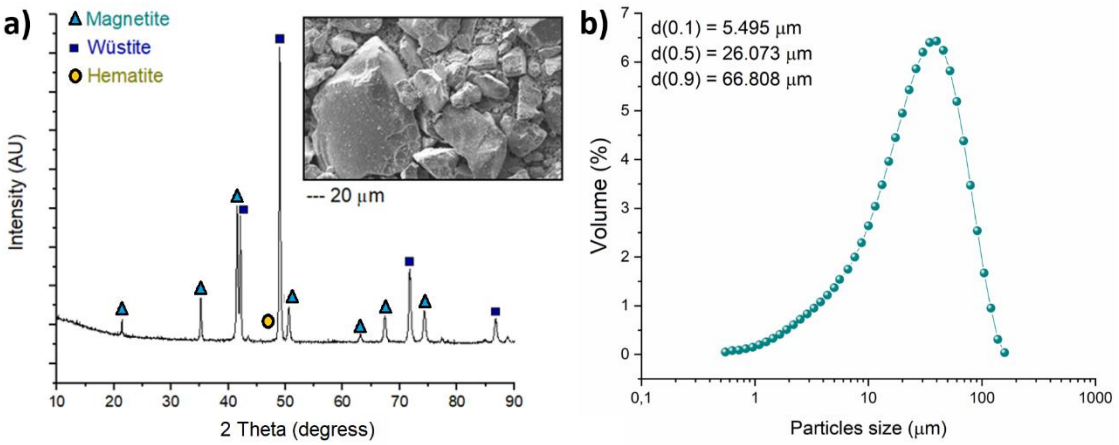

Fig. 3. a) Morphology and XRD pattern of mill scale powder, b) particle size distribution of mill scale powder.

3.2. DSC analysis

Fig. 4 depicts DSC curves of Al alloy, mill scale and Al-1%MS. Xiang Zhou et al [**18**], found that inert (Ar or N_2) atmosphere does not guarantee the absence of oxidation reaction in thermite reaction (traces of O_2 could be present in the chamber), which could explain peak number 1

attributed to the oxidation of Fe_3O_4 to Fe_2O_3. Peak number 2 appears at 577 °C in the 1% sample and does not appear in Al and mill scale. This temperature is between 525 °C [**18**] and 595 °C [**19**], widely recognized as that of the solid-state reaction between Al and Fe_2O_3, which is the thermite reaction mentioned in section 1.3.

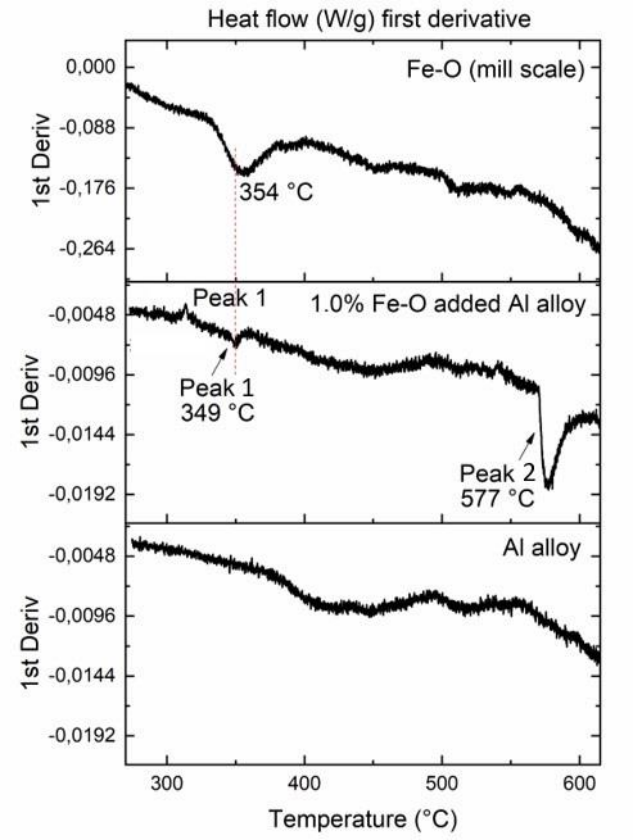

Fig. 4. DSC curves (first derivate) of Al-0% and Al-1% mill scale

3.3. Sintered samples

3.3.1. XRD analysis

Fig. 5 shows the XRD pattern of the sintered samples. The typical four peaks of aluminum (pdf 00-004-0787 of X'Pert HighScore) and the six peaks related to alumina (pdf 00-042-1468 of X'Pert HighScore) can be observed, as in the XRD diffractogram of the powders (**Fig. 2**). A wüstite (FeO)-diffracted peak was also observed, located at 42.1° (pdf 01-089-0686 of X'Pert HighScore). This last of these corresponds to the iron oxide particles. However, some extra peaks were observed after the sintering process. These showed the presence of iron aluminides (Fe-Al and

Fe-rich Al-Si), which indicates that the iron oxide particles were chemically reduced by the aluminum, as shown by DSC analysis, and that a solid solution between the aluminum and reduced iron had been formed. The peak located at 45.67° probably corresponds to an intermetallic compound of Fe-Al, of an approximate chemical composition of $Fe_{0.6}Al_{0.4}$ [**20**, **21**]. This phase probably also contains Si [**22**]. The peak located at 67.25° probably corresponds to an iron-rich aluminum silicon alloy [**23**].

As mentioned by other researchers [**14**], the chemical composition of the reaction products depends on the reaction extent and cooling conditions. The typical products include a metallic phase (such as metallic iron and intermetallics between iron and aluminum) and a ceramic phase, which involves alumina, Al_2O_3. These products were observed in this case.

The lattice parameters and crystallite size values were extracted from the XRD patterns. This information can be observed in **Table 1**. The samples exhibited similar lattice parameter and crystallite size values. When compared to crystallographic information of the aluminum powder, it was noted that the lattice parameter of the samples was higher, and the crystallite size was smaller. This means that internal stresses were released during the sintering process. The smaller crystallite sizes could indicate a recrystallization of the grains during the sintering process. This was expected, since during the grinding process the aluminum was subjected to cold work, and so an increase in the dislocation density is anticipated [24].

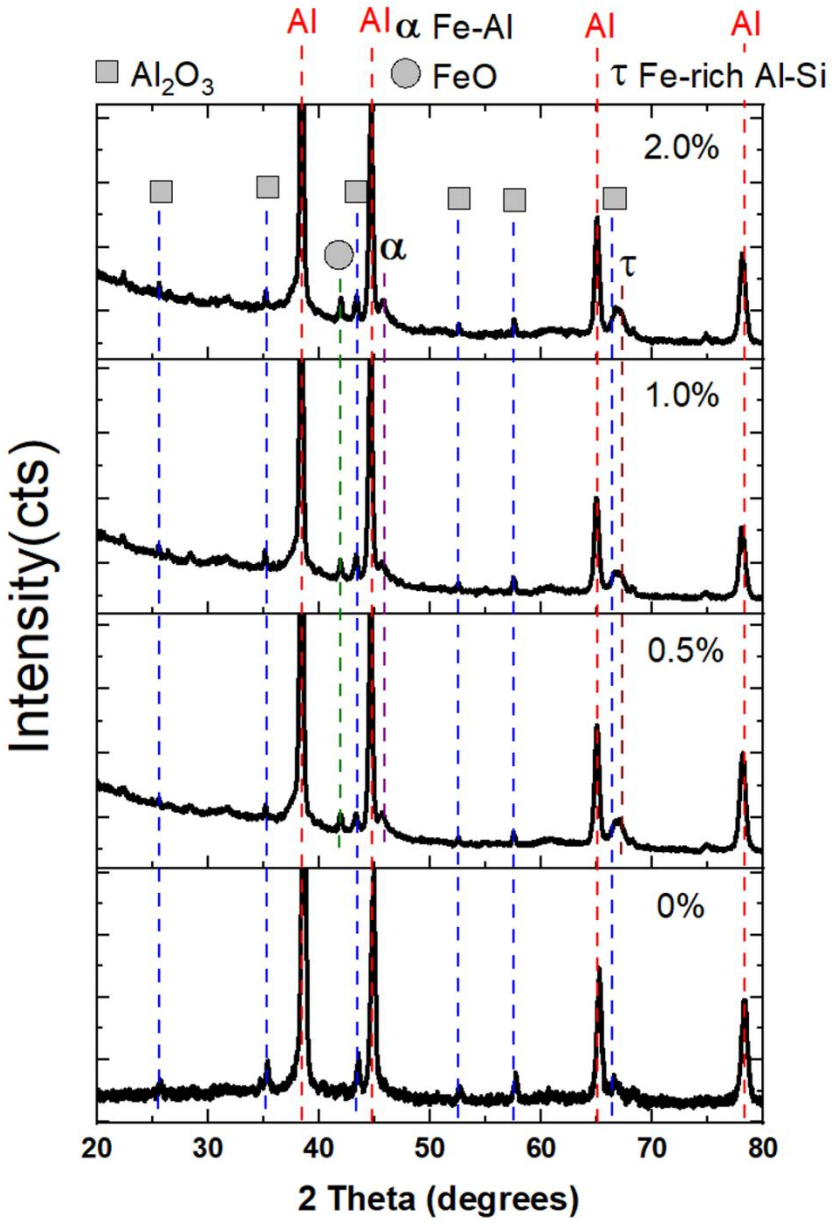

Fig. 5. XRD pattern of the sintered samples.

Table 1 Crystallographic information of sintered composites

Samples	Lattice parameters (nm)	Crystallite sizes (nm)
0.0% MS	0.40529 ± 0.00006	37.2
0.5% MS	0.40551 ± 0.00005	33.4
1.0% MS	0.40560 ± 0.00008	24.2
2.0% MS	0.40560 ± 0.00002	27.5

3.3.2.Microscopy and EDS

Micrographs of the 1.0% and 2.0% MS samples are shown in **Fig. 6** and **Fig. 7**, respectively. Black parts of the structure, corresponding to porosity, can be seen. In the case of the sample with 0.5% MS, non-interface was observed at that magnification. For the 1.0% MS sample, a clear interface between the iron oxide particles and the aluminum matrix was observed, and the iron oxide particle appears to be partially reduced. The kind of interface changed when 2.0% of MS was added, as shown in **Fig. 7**, where partially - reduced oxide particles are also observed, but an additional darker zone appears. The chemical composition was determined by EDS.

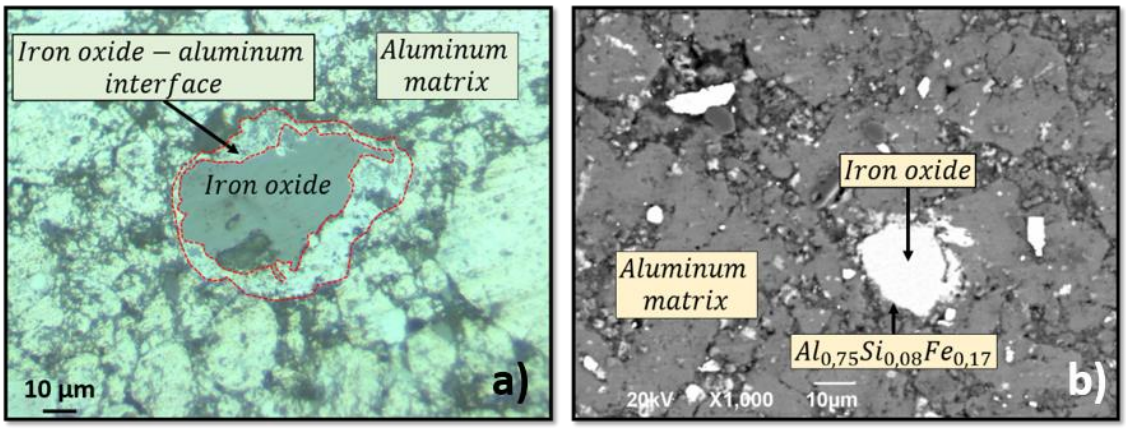

Fig. 6. Microstructure of samples with 1.0% of iron oxide by optical microscopy a), and scanning electron microscopy b).

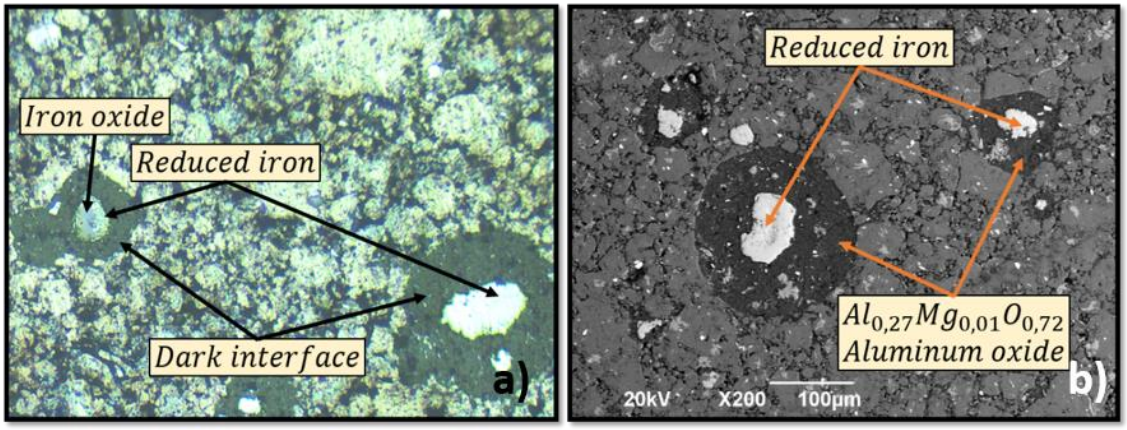

Fig. 7. Optical micrographs (500X): Dark interface between an iron oxide particle with the aluminum matrix, indicating partial chemical reduction of the iron oxide particles in the 2.0% MS sample.

The EDS measurement showed that the darker zone of the 2.0% MS sample was composed of aluminum oxide with traces of magnesium. The reduced part of the mill scale particle consisted of an aluminum-iron solid solution or an iron aluminide with traces of silicon. Cracks were observed in the aluminum oxide phase, which is expected to diminish the mechanical properties of the material. It was evident that, with higher iron oxide content in the material, the reducibility of the iron oxide increased, forming an alumina phase surrounding the Fe-Al intermetallic particles, which were fragile and contained cracks.

Chemical reactions involved in the process are represented by these chemical equations:

$$3Fe_2O_3 + 4Al \rightarrow 2Al_2O_3 + 6Fe + Heat$$

$$3FeO + 2Al \rightarrow Al_2O_3 + 3Fe + Heat$$

$$3Fe_3O_4 + 8Al \rightarrow 4Al_2O_3 + 9Fe + Heat$$

The process starts in the surface of the mill scale particle, forming metallic or intermetallic Fe-Al, and $FeAl_2O_4$ or Al_2O_3, as schematized in **Fig. 8**. Black arrows indicate heat diffusion.

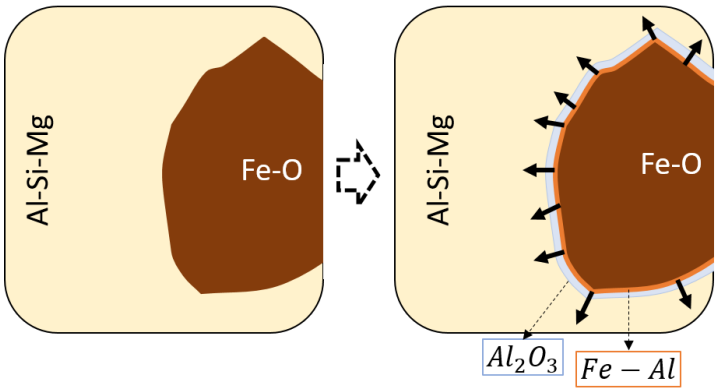

Fig. 8. Scheme of the chemical reduction of iron oxides by aluminum.

As can be seen in the chemical equations, the reactions generate heat. The reaction between aluminum and iron oxides is highly exothermic, and the amount of released heat could have been enough to melt aluminum. As recorded in the literature [**14**], a chemical reaction between hematite and aluminum generates $851.5\,\frac{kJ}{mol\ Al}$. It is expected that, with a low amount of mill scale, the heat produced in the chemical reduction reaction would rapidly dissipate throughout the matrix. However, with higher iron oxide content, it is expected that more heat would be produced inside the material and would not dissipate as quickly in the matrix. This heat could be enough to melt the aluminum surrounding the iron oxide particles, which can be easily oxidized and could produce the observed alumina. The oxygen is taken from the iron oxide particle, which proceeds to be reduced.

This reaction is considered a self-propagating high temperature process and it is obvious that the kind of interface between the iron oxide particles and the aluminum matrix formed is dependent on the diffusivity of the species and amount of heat released. It appears that the higher the quantity of iron oxide particles, the higher the presence of alumina in the interface. This is because of the increase in heat produced in the chemical reaction.

3.3.3.Hardness

Fig. 9 shows the behavior of hardness according to the content of iron oxide particles. As observed, there was a reinforcing effect with low contents of mill scale, and the highest hardness

was observed using 0.5% of mill scale. Beyond that value, the hardness diminishes. The thermite reaction was important in the formation of the interface between the matrix and the reinforcing particles. However, with higher amounts of mill scale, the release of heat due to the thermite reaction accelerated the reaction, which was self-propagating and increased the size of the interface of $FeAl_2O_4$ or Al_2O_3. This oxide interface cracked, causing the drop in hardness, as can be seen in SEM images.

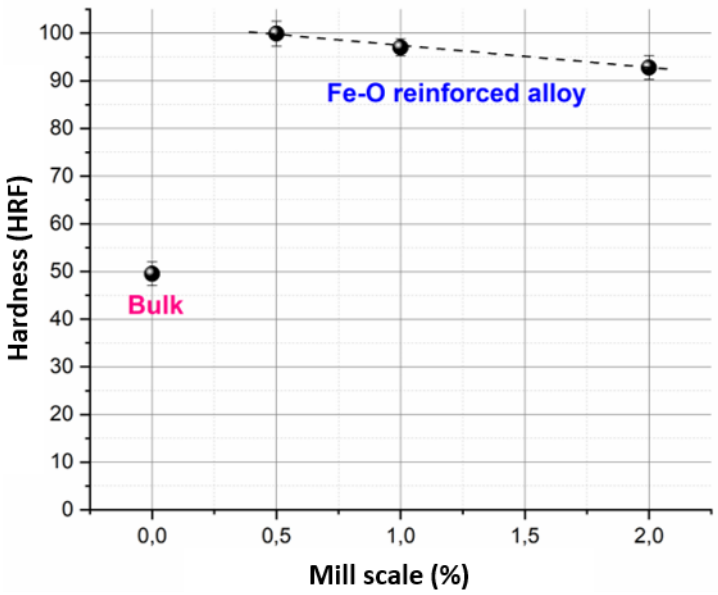

Fig. 9. Hardness behavior according to iron oxide content.

3.3.4. Corrosion

Representative Tafel curves of Al-0MS and Al-0.5%MS samples are shown in Fig. 10. It can be seen that the Galvanic potential of the Al-0.5%MS composite is about -0.971 V. The 6xxx Al alloy without mill scale shows a more negative Galvanic potential of -1.296 V, which means that the Al-0MS is more sensitive to the corrosion medium. The corrosion current density of Al-0MS was calculated as 45.60 µm/cm^2. The value obtained for Al-0.5%MS was as low as 1.93 µm/cm^2. The corrosion rates were of 496.7 µm/year and 21.0 µm/year for Al-0MS and Al-0.5%MS, respectively, which means that the corrosion rate is 23 times slower in the alloy without addition of mill scale. This trend is similar to that reported by M. Sunil Kumar et al [**25**], who made Al-

hematite composites by casting and found that the corrosion rate diminishes with the addition of hematite (adding hematite from 0 to 12% wt.). The explanation reported by A. Shivaramakrishna et al [**26**], who evaluated the corrosion characteristics of Fe_3O_4 – Al matrix composites in 3.5 % wt. NaCl, is that the iron oxide reinforcement particles act as an insulator and remain inert in the corrosion medium during the test. This means that the presence of iron oxide in the composites decreases the corrosion rate, reducing the exposure area of the alloy. This behavior is also observed with other particle reinforcements, such as when Si_3N_4 is added to AA8011 aluminum alloy [**27**]. In our case, however, besides iron oxide, XRD patterns showed Fe-Al and Fe-Al-Si intermetallic phases (Fig. 5). Although it has been found that intermetallics such as AlFeSi show that the initial open circuit potential more positive than that of Al matrix, leading to cathodic behavior against Al and, in turn to the dissolution of the Al around the intermetallic phase [**28**], in our case the quantity of this intermetallic phase is not enough to diminish the corrosion rate of the material.

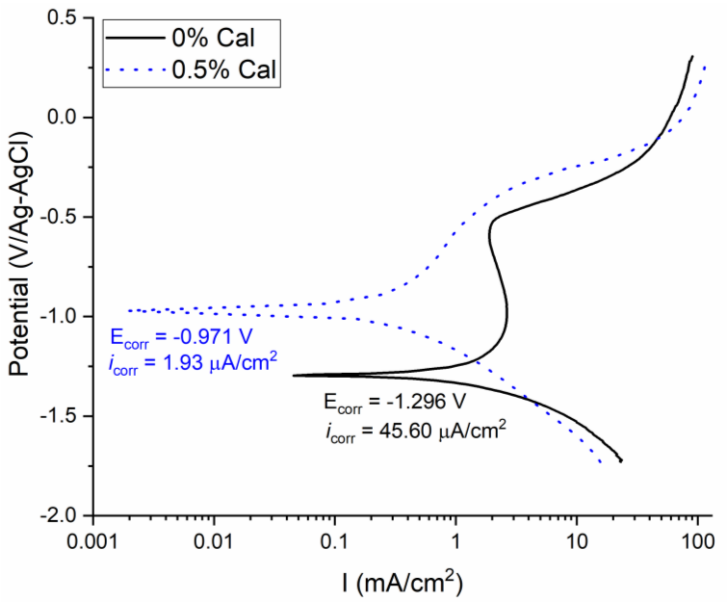

Fig. 10. Representative Tafel curves of Al and Al-0.5%MS

4. Conclusions

Following the 17th Sustainable Development Goal, a partnership between two research groups from Colombia and the UK was established to evaluate whether it is possible to manufacture a composite of aluminum saw chips and mill scale by-products using powder metallurgy techniques. Based on this study, it was concluded that:

- Aluminum and mill scale industrial by-products can be manufactured by powder metallurgy techniques to produce aluminum-iron oxide composites.
- Mill scale has a reinforcing effect on aluminum up to 0.5%. Beyond that value, hardness diminishes.
- Aluminum and iron oxide particles chemically react due to a thermite reaction, which is exothermic.
- The amount of mill scale added determines the kind of interface between the aluminum matrix and the iron oxide particles. Higher quantities of mill scale generate higher quantities of heat, which generates a fragile interface, leading to a reduction in hardness.
- 0.5% mill scale enhances hardness from 50.0 HRF, corresponding to bulk Al-0MS, to 99.9 HRF in pieces obtained by powder metallurgy using powder obtained by grinding Al chips.
- Addition of 0.5% mill scale to 6xxx Al alloy pieces obtained by powder metallurgy using powder obtained by grinding Al chips diminishes the corrosion rate from 496.7 µm/year to 21.0 µm/year.

5. Future research

This research is framed within a larger study, in which the next step is to evaluate the processability of the material by additive manufacturing techniques, specifically selective laser melting.

Acknowledgment

The authors would like to thank the Royal Academy of Engineering for co-financing the project, as well as Cardiff University and the Colombian School of Engineering Julio Garavito.

Conflict of interest

The authors declare that they have no conflict of interest

References

1. Goal 12: Ensure sustainable consumption and production patterns, United Nations. Online, February 2023: https://www.un.org/sustainabledevelopment/sustainable-consumption-production/
2. Política Nacional de Producción y Consumo Sostenible. Online, February 2020: https://www.rds.org.co/es/recursos/politica-nacional-de-produccion-y-consumo-sostenible
3. O. A. Zambrano, J. J. Coronado, S. A. Rodríguez, Surf. Coat. Technol. 282, 155 (2015). https://doi.org/10.1016/j.surfcoat.2015.10.028
4. Mill Scale Sourcing. Online, January 2023: https://millscale.org/
5. J. Gronastajsky, H. Marciniak, A. Matuzak, J. Mater. Process. Technol. 106, 34 (2000). https://doi.org/10.1016/S0924-0136(00)00634-8
6. J. Gronastajsky, A. Matuzak, J. Mater. Process. Technol. 92-93, 35 (1999). https://doi.org/10.1016/S0924-0136(99)00166-1
7. L. M. Rojas-Díaz, L. E. Verano-Jiménez, E. Muñoz-García, J. Esguerra-Arce, A. Esguerra-Arce, Powder Technol. 360, 301 (2020). https://doi.org/10.1016/j.powtec.2019.10.028
8. S. P. Shivakumar, A. S. Sharan, K. Sadashivappa, Appl. Mech. Mater. 895, 122 (2019). https://doi.org/10.4028/www.scientific.net/AMM.895.122
9. E. Bayraktar, F. Ayari, M. J. Tan, A. Tosun-Bayraktar, D. Katundi, J. Achiev. Metall. Mater. Trans B. 45, 352 (2010). https://doi.org/10.1007/s11663-013-9970-1

10. Z. Nissara, A. Kazib, M. Safiullac, M. Faisald, Mater Today: Proceedings 4, 11999 (2017). https://doi.org/10.1016/j.matpr.2017.09.122
11. V. Suresh, P. Vikram, R. Palanivel, R. F. Laubscher, Mater Today: Proceedings 5, 27852 (2018). https://doi.org/10.1016/j.matpr.2018.10.023
12. C. Puncreobutr, P. D. Lee, K. M. Kareh, T. Connolley, J. L. Fife, A. B. Phillion, Acta Mater. 68, 42 (2014). https://doi.org/10.1016/j.actamat.2014.01.007
13. L. Lu, A. K. Dahle, Metall. Mater. Trans. A. 36, 819 (2005). https://doi.org/10.1007/s11661-005-1012-4
14. L. Duraes, B. F. O. Costa, R. Santos, A. Correia, J. Campos, A. Portugal, Mater. Sci. Eng. A 465, 199 (2007). https://doi.org/10.1016/j.msea.2007.03.063
15. D. Prabhu, P. Rao, J. Environ. Chem. Eng. 1, 676 (2013). http://dx.doi.org/10.1016/j.jece.2013.07.004
16. V. Shrivastava, G. K Gupta, I. B. Singh, J. Alloys Compd. 775, 628 (2019). https://doi.org/10.1016/j.jallcom.2018.10.111
17. T. Khelfa, M. A. Rekik, M. Khitouni, J. M. Cabrera-Marrero, Int. J. Adv. Manuf. Technol. 92, 1731 (2017). https://doi.org/10.1007/s00170-017-0282-5
18. X. Zhou, Y. Zhu, X. Ke, K. Zhang. J. Mater. Sci. 54, 4115 (2019). https://doi.org/10.1007/s10853-018-3094-6
19. P. Thakur, V. Sharma, N. Thakur. Physica B. Condens 610, 412803 (2021). https://doi.org/10.1016/j.physb.2020.412803
20. A. J. Panas, C. Senderowski, B. Fikus, Thermochim. Acta 676, 164 (2019). https://doi.org/10.1016/j.tca.2019.04.009
21. M. Rank, P. Gotcu, P. Franke, H. J. Seifert, Intermetallics 94, 73 (2018). https://doi.org/10.1016/j.intermet.2017.12.015
22. T. Gao, Y. Bian, K. Hu, K. Zhao, W. Zhang, X. Liu, Results in Materials 3, 100036 (2019). https://doi.org/10.1016/j.rinma.2019.100036

23. X. Wu, H. Zhang, Z. Ma, T. Tao, J. Gui, W. Song, B. Yang, H. Zhang, J. Alloys Compd. 786, 205 (2019). https://doi.org/10.1016/j.jallcom.2019.01.352

24. P. A. Pulido-Suárez, K. S. Uñate-González, J. G. Tirado-González, A. Esguerra-Arce, J. Esguerra-Arce, J. Mater. Res. Technol. 9, 11769 (2020). https://doi.org/10.1016/j.jmrt.2020.08.045

25. M. Sunil Kumar, N. Sathisha, T.R. Rajesh, Mater Today, 66, 1598 (2022). https://doi.org/10.1016/j.matpr.2022.05.247

26. A. Shivaramakrishna, Y. Basavara, R. Subramanya, Int. J. Cast Met. Res. 35, 51 (2022). https://doi.org/10.1080/13640461.2022.2078551

27. J. Fayomi, A.P.I. Popoola, O.M. Popoola, O.S.I. Fayomi, Phys.: Conf. Ser. 1378, 42054 (2019). doi:10.1088/1742-6596/1378/4/042054

28. X. M. Chen, Q. P. Dong, Z. G. Liu, X. N. Wang, Q. Y. Zhang, Z. R. Hu, H. Nagaumi, J. Mater. Res. Technol. 9 (6), 16116 (2020). https://doi.org/10.1016/j.jmrt.2020.11.077